Supplementary Material for

New Geochemical Framework and Geographic Information System Methodologies to Assess Element Occurrence and Persistence in Groundwater and Surface Water

Johanna M. Blake [1,*], Katherine Walton-Day [2], Tanya J. Gallegos [3], Douglas B. Yager [4], Andrew Teeple [5], Delbert Humberson [6], Victoria Stengel [5] and Kent Becher [7]

[1] New Mexico Water Science Center, U.S. Geological Survey, Albuquerque, NM 87113, USA
[2] Colorado Water Science Center, U.S. Geological Survey, Lakewood, CO 80215, USA; kwaltond@usgs.gov
[3] Geology, Energy, and Minerals Science Center, U.S. Geological Survey, Reston, VA 20192, USA; tgallegos@usgs.gov
[4] Geology, Geophysics, and Geochemistry Science Center, U.S. Geological Survey, Denver, CO 80225, USA; dyager@usgs.gov
[5] Oklahoma-Texas Water Science Center, U.S. Geological Survey, Austin, TX 78754, USA; apteeple@usgs.gov (A.T.); vstengel@usgs.gov (V.S.)
[6] Water Accounting Division, International Boundary and Water Commission, El Paso, TX 79922, USA; delbert.humberson@ibwc.gov
[7] Retired, Oklahoma-Texas Water Science Center, U.S. Geological Survey, Austin, TX, 78754, USA; kentbecher@sbcglobal.net
* Correspondence: jmtblake@usgs.gov

Two cross sections along the Texas Coastal Plain, from the Houston and Rio Grande embayments, are shown in Figure S1.

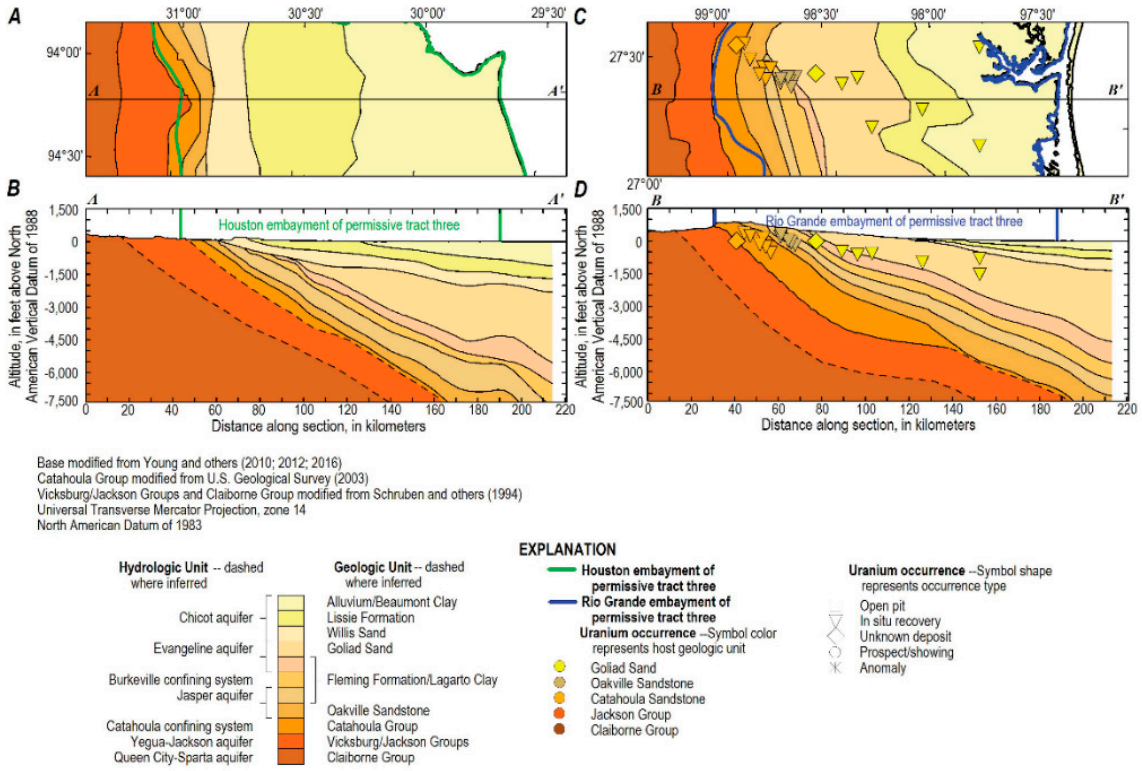

Figure S1. A. Generalized map and B. geologic cross section A-A′ and C. generalized map and D. geologic cross section B-B′ in the South Texas Coastal Plain.

1. Geochemical and Physical Conditions Controlling Mobility of Elements

Aqueous complexation and adsorption competition can affect the behavior of metals in water. A complex is the dissolved association of a cation and anion or neutral molecule [1]. Competition occurs when more than one ion can fit on a sorption site such as Fe-(hydr)oxides. The competing ion can replace the desorbed ion [1]. Alkalinity, generally as bicarbonate or carbonate, is found at a range of concentrations in groundwater and surface water and can contribute to complexation or competition [2]. In addition to providing information about buffering capacity and pH, alkalinity can influence formation of aqueous metal complexes involving U and As among other co-occurring elements [3,4]. It is well established that U(VI) forms aqueous complexes as uranyl-carbonates, which can dominate the U behavior in water [4,5,6]. Arsenic (3) tends to form carbonate complexes while As(5) does not [7]. In addition, bicarbonate and phosphate can compete with As for sorption sites on Fe-(hydr)oxides [2]. If this occurs, As can be released from the solid and become mobile.

Iron substrates in the environment can include hydrous ferric oxides including amorphous ferric hydroxide, amorphous iron oxyhydroxide, and ferrihydrite as well as goethite, the crystalline oxide form. These substrates are ubiquitous in the environment and are often the primary sorbent for metals [8,9]. Iron oxides are typically found as secondary minerals that form from weathering of primary minerals [9]. Metal substrates can occur as coatings on clay-size minerals in soils and sediments or as minerals [9]. Sorption of constituents of potential concern (COPCs) to iron substrates is pH and redox dependent [9].

Hydrogen sulfide (H_2S) and related species can have a physiochemical effect on mobility by affecting the redox state of the water and water-rock interaction. A common reductant associated with the South Texas Coastal Plain roll-front deposits is "sour gas" (methane + hydrogen sulfide) that migrated along faults into ore-bearing formations from hydrocarbon environments deeper in the subsurface [10,11,12]. The existence of reduced sulfur can lead to sulfide precipitates containing elements such as As, Fe, Mo, U, Se, and V [13]. Uranium deposits in this region were also reduced by pyrite-rich geochemical cells formed around paleo-organic-rich lagoons and marshes [12].

Table S1 provides a simplified list of expected geochemical mechanisms associated with the COPCs based on speciation, redox, pH, Fe substrates and H_2S. The information was compiled from the literature and does not necessarily encompass every detail of the possible geochemical mechanisms but focused on the specific questions discussed in this study.

Table S1. Geochemical mechanisms associated with constituents of concern.

Element	Form in water (oxyanion, oxycation or complex)	Species	Effect from pH	Effect from redox	Relation to Fe oxides	Relation to H2S	Forms Sulfides	References
As	AsO_4^{3-}, H2AsO4-, HAsO4-2	As(V)	increase in pH(>8.5) desorption from Fe-oxides; below pH 5-6, sorption to Fe oxides; mobilized at high pH.	reduce to As(III); reductive dissolution of iron oxyhdroxide phases	couples with iron oxides	Can form solids with iron and sulfide	X	Plant et al., 1996; Dixit and Hering, 2003; McMahon and Chapelle, 2008; Smedley and Kinniburgh, 2002; Nicot et al., 2010; Kirk et al., 2010
	AsO_3^{3-}, H3AsO3, H2AsO3-	As(III)	pH greater than 7-8, sorbs to Fe oxides; at neutral pH As(III) can desorb from mineral oxides	oxidize to As(V)	Sorbs above pH 7-8	Can form solids with iron and sulfide		Smedley and Kinniburgh, 2002; Dixit and Hering, 2003; Kirk et al., 2010
V	Vanadate (H_3VO_3; $H_2VO^-_4$ and HVO^{2-}_4)	V(V)	increase in pH(>8.5) results in desorption from Fe-oxides	mobile in oxic conditions	sorbs until pH greater than 8.5		X	McMahon and Chapelle, 2008; Nicot et al., 2010; Wright and Belitz, 2010; Mochizuki et al., 2018
	VO^{2+} and $V(OH)^+_3$	V(IV)	mobile in acidic conditions	only exists in conditions more reducing than that of the gulf coast; mobile under reducing conditions				Nicot et al., 2010; Wright and Belitz, 2010
Mo	MoO4-, H2MoO4	Mo(VI)	increase in pH(>8.5) desorption from Fe-oxides; mobile at pH greater than 7	mobile in oxic conditions	sorbs until pH of 8.5	Can form solids with iron and sulfide	X	Plant et al., 1996; McMahon and Chapelle, 2008; Nicot et al., 2010; Migeon et al., 2020
		Mo(IV)	Mobile at high ph			fairly insoluble as		Plant et al., 1996

		Se(-II)	anoxic			molybdenite (MOS2)		
Se	selenate, H2SeO4, SeO4-2, HSeO4-	Se(VI)	increase in pH(>8.5) desorption from Fe-oxides	mobile in oxic conditions	sorbs to Fe-oxides	reduction in the presence of iron sulfides; can sorb to iron sulfides	X	Plant et al., 1996; McMahon and Chapelle, 2008; Nicot et al., 2010; Mitchell et al., 2013
	selenite H2SeO3, HSeO3-, SeO3-2	Se(IV)	mobile at high pH	insoluble and precipitates under mildly reducing conditions	selenite sorbs to Fe-oxides	reduction in the presence of iron sulfides; can sorb to iron sulfides		Mitchell et al., 2013; Plant et al., 2014; Etteieb et al., 2020
	UO_2^{2+}, U(OH)4, U(OH)3+	U(IV)	increase in pH(>8.5) desorption from Fe-oxides	reducing conditions, immobile	sorbs to Fe-oxides	can form sulfide precipitates		Plant et al., 1996; Smith, 2007; McMahon and Chapelle, 2008; Nicot et al., 2010
U	UO_2^{2+}	U(VI)		oxic conditions, mobile	sorbs to Fe-oxides		X	Fox et al., 2006; Smith, 2007
	Uranyl-carbonate complexes ($UO_2(CO_3)_2^{2-}$ and $UO_2(CO_3)_3^{4-}$), UO2CO3	U(VI)	mobile in circumneutral to alkaline pH	mobile in oxic conditions				Fox et al., 2006; Stewart et al., 2010
	Calcium-uranyl-carbonate complexes ($Ca_2UO_2(CO_3)_3^0$(aq); $CaUO_2(CO_3)_3^{2-}$)	U(VI)	mobile at alkaline pH	mobile in oxic conditions				Fox et al., 2006; Stewart et al., 2010

2. Evaluate the Distribution of Master Variables

In the Smith (2007) framework, pH and general redox conditions (oxic/anoxic) are primary controlling factors used to categorize mobility (very mobile, mobile, somewhat mobile, and scarcely mobile to immobile) of multiple chemical elements in water. The presence or absence of oxidized iron substrates is an additional factor used to partition chemical mobility among elements because sorption of many elements to oxidized iron substrates limits their mobility [13]. In addition, the Smith method considered the presence or absence of hydrogen sulfide to categorize element mobility because precipitation of sulfide minerals limits the mobility of multiple trace elements. Smith (2007 [13]) states that the mobility classification … "should be used only in a relative sense and does not provide any information about absolute concentrations or quantitative data" and that to use the approach, "in a natural setting, it is necessary to have a good grasp of geochemical conditions" (p. 29). Because of these considerations and because Smith (2007 [13]) focused on surface water and the geochemical framework developed in the work described herein evaluated geochemical mobility in both groundwater and surface water, we modified the Smith (2007 [13]) mobility categories by incorporating some other geochemical methods and considerations typical of groundwater. In particular, we incorporated the pH cutoffs of the geochemical barriers from Perel'man (1986 [14]). To identify the redox condition for each sample, we used a redox toolbox developed by Jurgens et al. (2009 [15]) for assigning the redox category for each sample. McMahon and Chapelle (2008 [16]) discuss the framework for the redox toolbox and apply it to principal aquifers in the United States. The master variables were evaluated in groundwater and surface water. Major rivers are shown in Figure S2. pH ranges are shown in Figure S3 and the redox indicators are shown in Table 2.

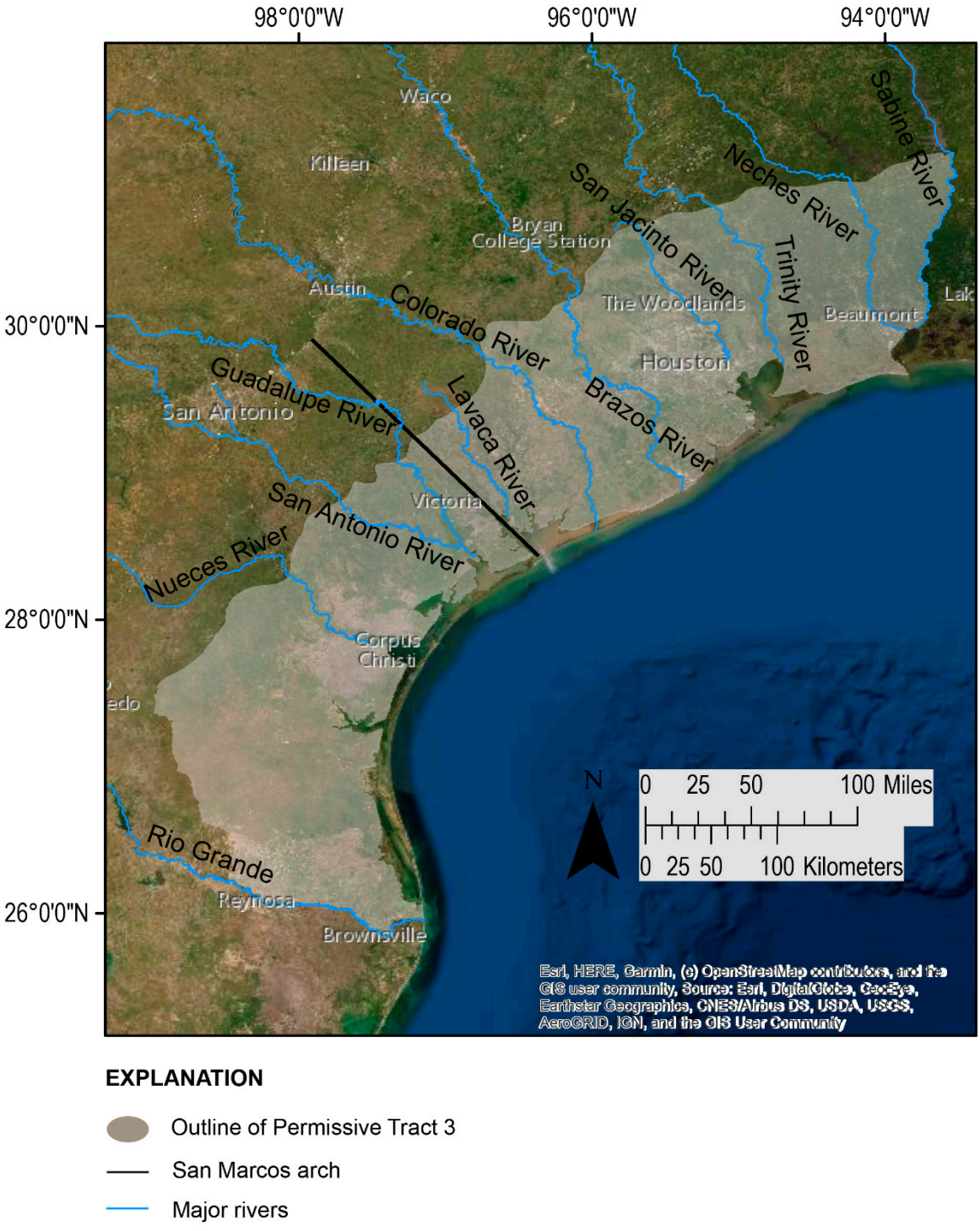

EXPLANATION

Outline of Permissive Tract 3

San Marcos arch

Major rivers

FigureS2. The major rivers in the Texas Coastal Plain shown in blue and locations of major cities shown in white. An outline of Permissive Tract 3 and the San Marcos arch are shown.

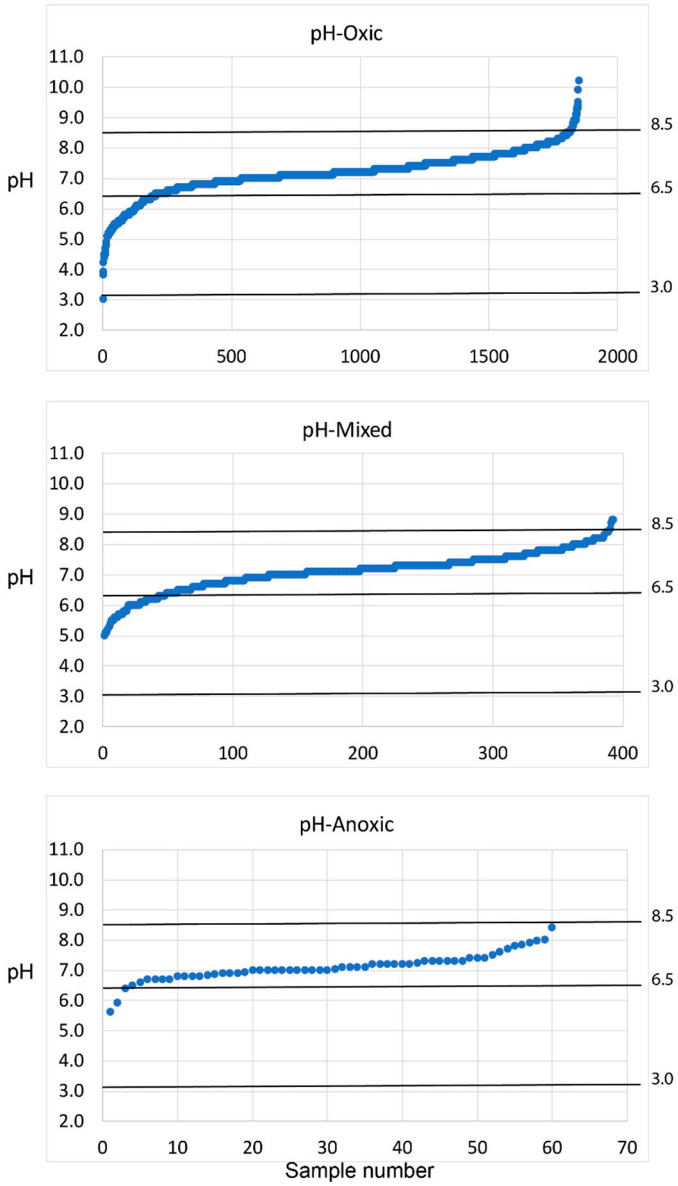

Figure S3. Graphs showing pH distribution from NURE groundwater data in each redox category (oxic, mixed, and anoxic), assigned using the Jurgens et al. (2009) redox calculator, by sample number.

Table S2. Electron acceptors and threshold concentrations used in the redox calculator (Jurgens et al., 2009).

Electron Acceptor	Threshold Concentration
Dissolved O_2	0.5 mg/L
NO_3^- (as Nitrogen)	0.5 mg/L
Mn^{2+}	50 µg/L
Fe^{2+}	100 µg/L
SO_4^{2}	0.5 mg/L

3. Redox Assumptions

To apply the redox framework in this study, there were several assumptions made based on the constituents reported in each dataset.

First, we confirmed that water samples were filtered or preserved (acidified) and were not otherwise treated or blended such that the data evaluated in this study are suitable for redox classification. The National Uranium Resource Evaluation (NURE) data from Permissive Tract 3 lists the sample treatment as "filtered with 0.45 μm filter in the laboratory" [17].

Second, in the published geochemical data used in this study, it was noted that the exact method of DO measurement (flow-through cell, bucket, or other) may not be known or a flow-through cell may not have been used. DO data are often included in datasets, but the value reported may be erroneous due to contamination associated with the measurement method used when sampling groundwater [18,19]. For instance, when the NURE samples were collected in 1973 to 1980 [17], flow-through cells were not routinely used and NURE methods indicated that DO was measured in waters collected in a bucket with a Horiba U-7 water analyzer [20,21,22].

The oxic/anoxic threshold for DO of Jurgens et al. (2009 [15]) was slightly modified for water samples identified as "mixed" as follows. Jurgens et al. (2009 [15]) suggests: "Samples that have dissolved O_2, but are missing one or more of the other four constituents, will have a general redox category of either "$O_2 \geq 0.5$ mg/L" or "$O_2 < 0.5$ mg/L". These two categories are used to distinguish between predominately oxic and anoxic conditions" [15]. However, given the sensitivity of DO measurements to atmospheric exposure and the slow response of DO electrodes below 1 mg/L [19], in this study, DO concentrations less than 1 mg/L suggested an anoxic environment. This assumption was only used for samples with a general redox category result of "mixed." That is, if the redox category assigned based on overall sample characteristics was mixed, and DO concentrations were less than 1 mg/L, then the redox assignment was manually changed to anoxic. This adjustment was made for 2.9% of the NURE groundwater data and 0% of the NURE surface-water data. In the NURE datasets, there were no DO data listed as below detection limit. However, if there was not a DO value for a sample, the value was left blank and the redox category was based on the other parameters. This situation occurred for 14% of the NURE groundwater data and 75% of the NURE surface-water data.

If DO was not reported, then dissolved Mn^{+2} and Fe^{2+} concentrations were used in order to establish the redox category. Dissolved Mn and Fe concentrations in water are generally reported as total concentrations without measuring the species of each, as in the NURE dataset. However, the redox framework uses Mn^{2+} and Fe^{2+} concentrations for defining the redox condition [15], and we needed to define what the most likely species of each was in our dissolved sample data. The most common form of dissolved Fe in groundwater is Fe^{2+} [23] especially in oxidizing conditions (p*e* 0 to 10) as Fe(II) solids are more soluble than Fe(III) solids [24]. Manganese follows a similar speciation pattern to that of Fe under environmental conditions where the reduced aqueous divalent form is more stable [23]. Mn(IV) and Fe(III) solids are generally insoluble at near neutral pH (6.5 to 8.5), which is the range in 86.9 % of the NURE groundwater data used in this study, and their precipitation limits the amount of oxidized species (Fe(III) and Mn (IV)) that occurs in water ([7], Figure S4) Although acidic conditions can produce measured concentrations of Mn^{4+} and Fe^{3+} [24,16], the data used in the study are not predominantly acidic (88.4% of the NURE groundwater data and 97.2% of the NURE surface-water data used in this study have a pH greater than 6.5).

P*e*-pH and speciation diagrams created in Geochemists Workbench (LLNL thermo database) (Bethke and Farrell, 2020 [25]) based on Mn and Fe thermodynamics (Figure S4a-d) (constructed using the low and high concentrations of Fe and Mn reported in our datasets of 1.79×10^{-7} mol/L and 1.63×10^{-5} mol/L Fe and 3.64×10^{-8} mol/L and 6.94×10^{-5} mol/L Mn) indicate that Fe^{2+} and Mn^{2+} are the dominant species found in solution across anoxic to oxic conditions (p*e* ranging from −8 to 10) and across a range of pH values (pH 3 to 12). Therefore, it can be assumed that total concentrations for Fe and Mn in the

datasets used in this study represent groundwater as Fe^{2+} and Mn^{2+} [16,23,26]. A conceptual pe-pH diagram is shown in Figure S5 and microbially mediated redox processes are shown in Figure S6. Figure S7 shows PHREEQC modeled saturation indices across pH for pyrite, goethite, hematite, magnetite, maghemite, jarosite, $Fe(OH)_3$(a), and $Fe_3(OH)_8$, $Fe(OH)_{2.7}Cl_{.3}$ calculated from NURE groundwater data. Graphs are separated by redox condition A. anoxic, pe= -8, B. mixed, pe= 0, and C. oxic, pe= +11.

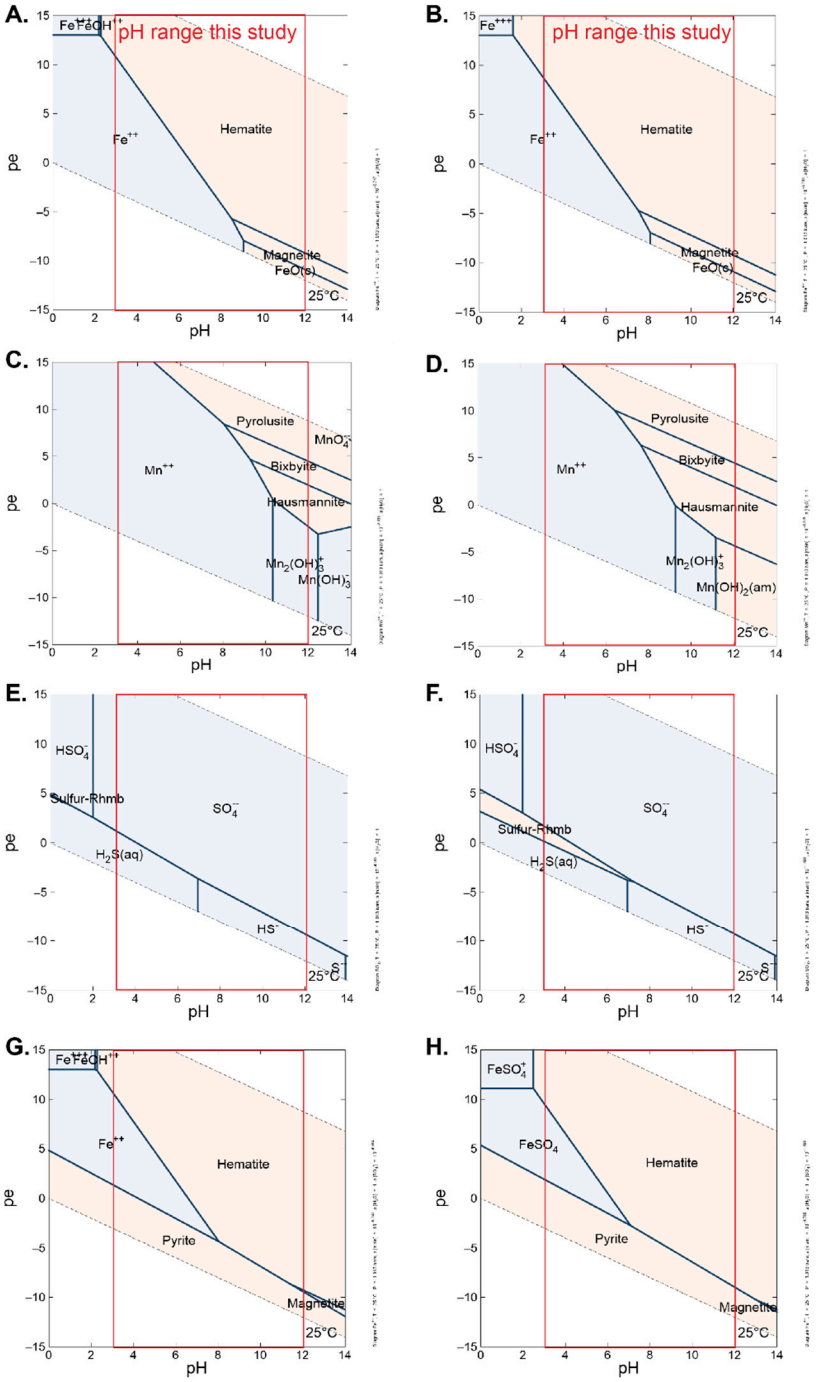

Figure S4. Pe-pH diagrams of **A**. Fe (1.79×10^{-7} mol/L), **B.** Fe (1.63×10^{-5} mol/L), **C.** Mn (3.64×10^{-8} mol/L), **D.** Mn (6.94×10^{-5} mol/L), **E.** SO_4^{2-} (2.60×10^{-5} mol/L), **F.** SO_4^{2-} (3.17×10^{-2} mol/L), **G.** Fe and SO_4^{2-} (1.79×10^{-7} mol/L and 2.60×10^{-5} mol/L), and **H**. Fe and SO_4^{2-} (1.63×10^{-5} mol/L and 3.17×10^{-2} mol/L). Element concentrations are the lowest and highest concentration in the NURE groundwater dataset. The pH range of the NURE groundwater dataset (3.0 to 12) is shown on each pe-pH diagram as a red box.

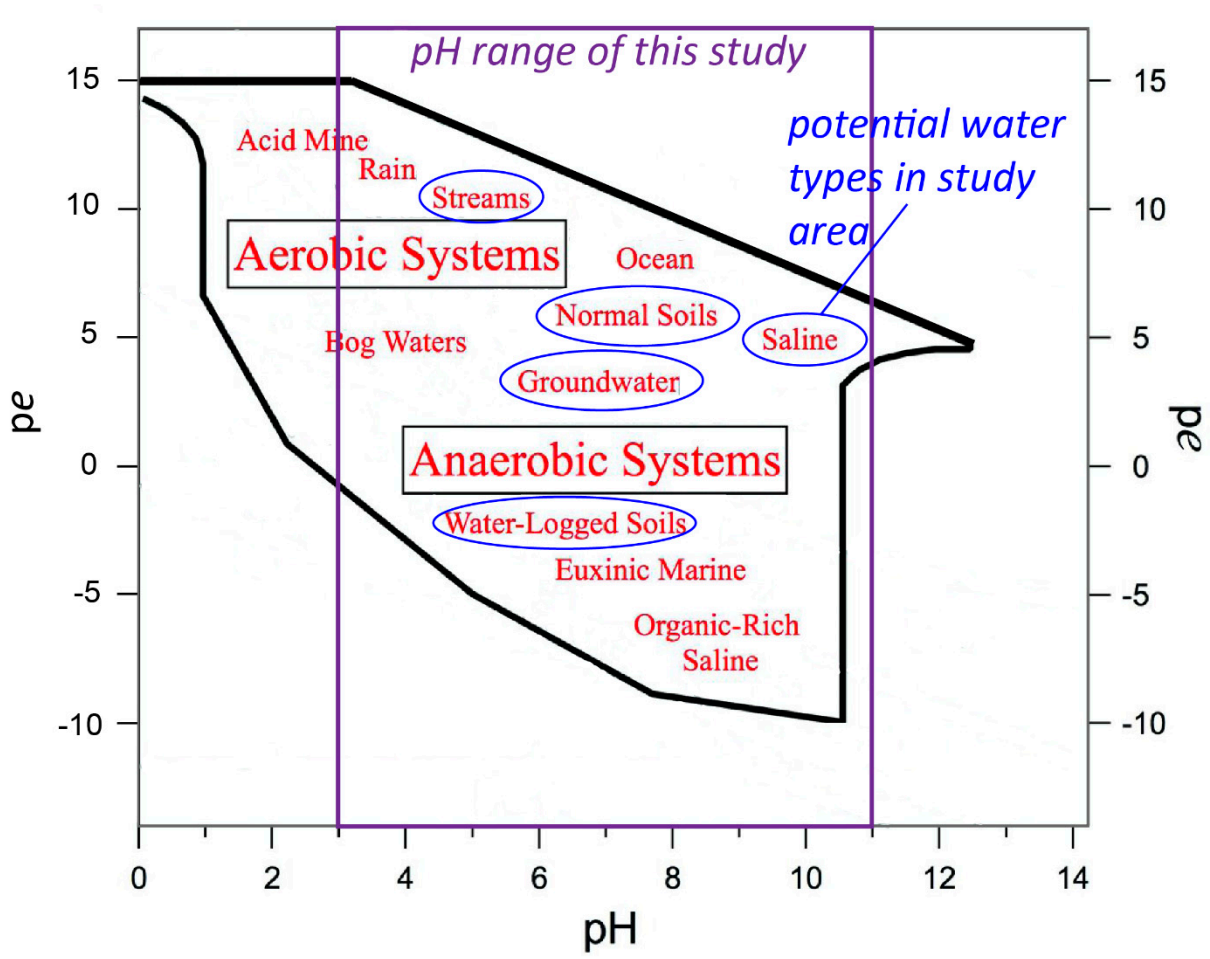

Figure S5. P*e*-pH diagram showing approximate regions of typical environmental systems (modified from Grundl et al., 2011 (27)). The purple box highlights the range of pH values in this study. The blue circles highlight potential water types in the study area.

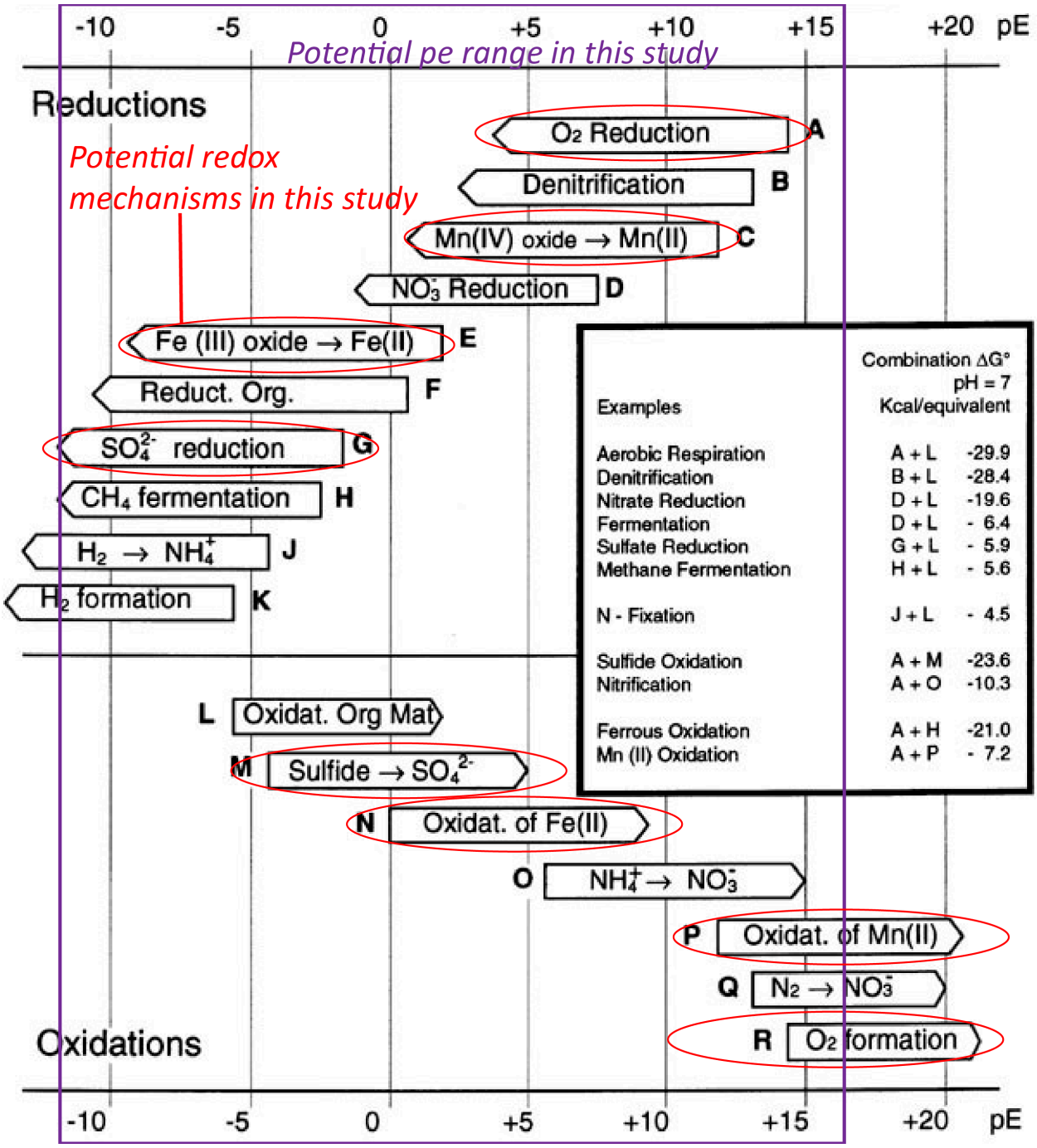

Figure S6. Sequence of microbially mediated redox processes (modified after Stumm and Morgan, 1981 (27)). The red ovals highlight potential redox processes occurring in the Texas Coastal Plain based on data available in NURE groundwater samples. The purple box highlights the potential range of p*e* values in the study area.

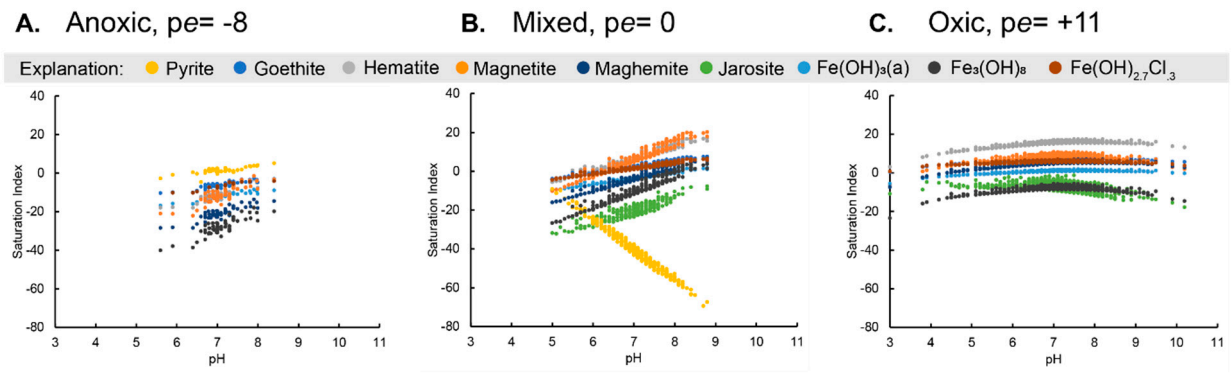

Figure S7. Saturation indices across pH for pyrite, goethite, hematite, magnetite, maghemite, jarosite, $Fe(OH)_3(a)$, and $Fe_3(OH)_8$, $Fe(OH)_{2.7}Cl_{.3}$ calculated from NURE groundwater data. Graphs are separated by redox condition A. anoxic, pe= -8, B. mixed, pe= 0, and C. oxic, pe= +11.

4. H_2S Assumptions

4.1. Hydrogen Sulfide Odor Reported

In our study (the NURE samples were collected from 1975 to 1980), measurements of dissolved sulfide were not explicitly reported. However, H_2S "odor" was sometimes reported. In the NURE groundwater dataset, an H_2S odor was reported for 222 of 2,302 samples. However, of the 222 samples with a reported H_2S "odor", the redox calculator defined only 14 as anoxic, 47 as mixed, and 161 as oxic. The fact that the H_2S "odor" does not directly correlate to redox condition may be because of the environment of the South Texas Coastal Plain where numerous anoxic or sub-oxic marshes and wetlands [29] exist and seeps of H_2S via faults above petroleum deposits have been identified [30]. In addition, along the South Texas Coastal Plain, salt domes contain liquid sulfur in the caprocks and H_2S smell has been noted (Figure S8;[31]). Regardless of the redox condition, the concentration of H_2S in groundwater could affect the precipitation of sulfide minerals.

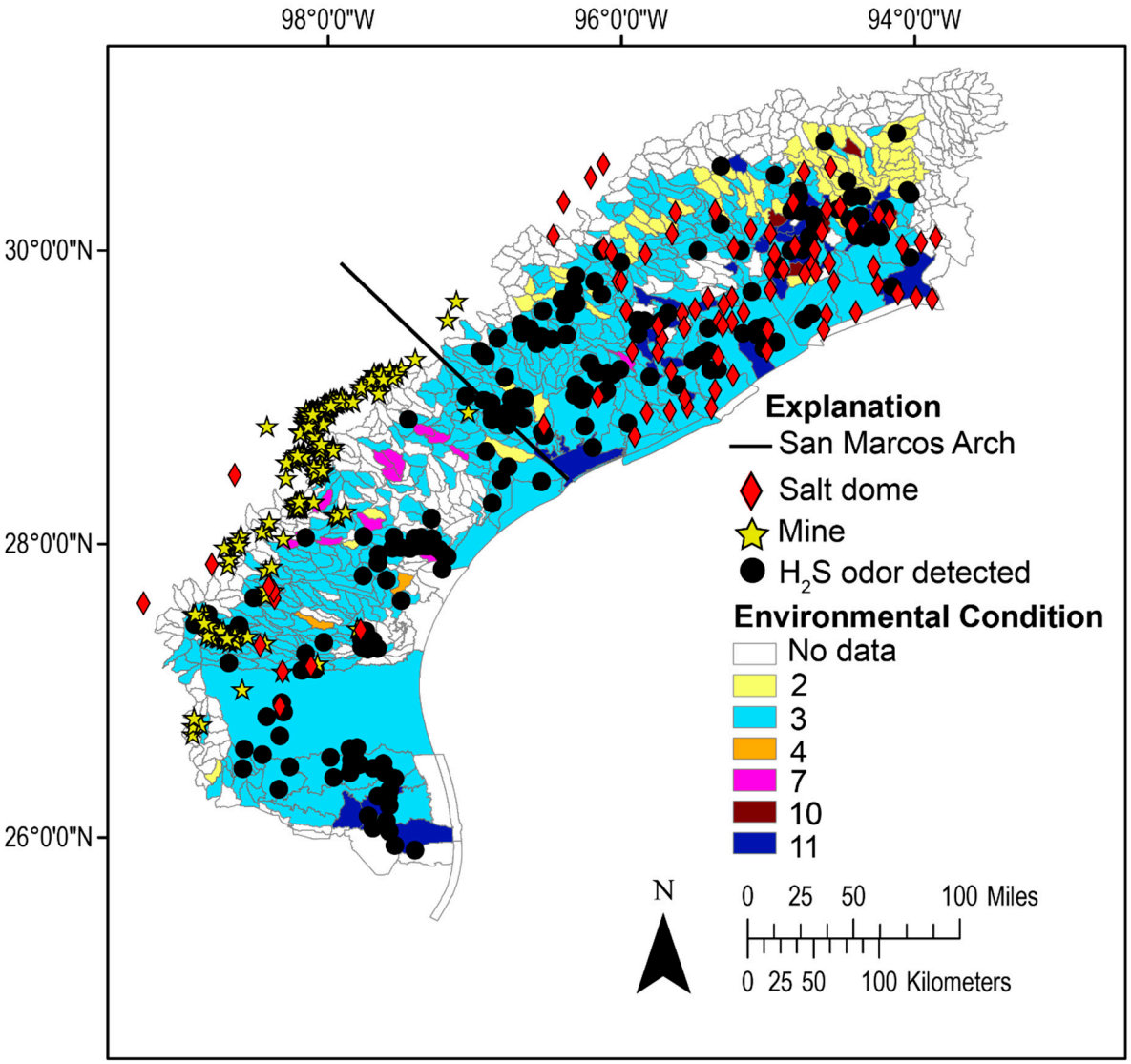

Figure S8. Location of salt domes, mines, and H_2S odor detected in NURE groundwater samples along the Texas Gulf Coast.

H_2S has a low odor threshold where the minimum perceptible (to humans) odor concentration in air is 0.13 ppm [32]. Henry's Law can be used to calculate the concentration of H_2S in water based on the gas concentration in air [33]. We did this to evaluate the potential concentration of H_2S in water. The Henry solubility (H^{cp}) can be defined as:

$$H^{cp} = C_a/p \quad (1)$$

where C_a is the concentration of a species in the aqueous phase and p is the partial pressure of that species in the gas phase under equilibrium (Sander, 2015).

The Henry solubility can also be expressed as a dimensionless ratio:

$$H^{cc} = C_a/C_g \quad (2)$$

where C_a is the concentration of a species in the aqueous phase and C_g is the concentration of the species in the gas phase. To convert from H^{cp} to H^{cc} for an ideal gas:

$$H^{cc} = H^{cp} \times RT \quad (3)$$

where R= the gas constant and T= temperature [33].

Table S3 shows the values for C_a, the concentration of H_2S in solution at the lowest concentration, 0.13 mg/L, humans can detect in air. The calculated C_a, based on a C_g of 0.13 mg/L, from Henry's Law is 9.23×10^{-6} mol/L, two orders of magnitude lower than the 10E-4 mol/L typical value reported by [1], though brines associated with petroleum or in interstitial waters in marine sediments may have higher concentrations [1].

Table S3. Henry's Law values and results of aqueous H_2S concentrations.

	Value	Units
H_{cp} for H_2S=	1.0×10^{-3}	$mol \cdot m^{-3} \cdot Pa^{-1}$
C_g=	0.13	$0.13\ mg \cdot L^{-1}$
C_g=	4.06×10^{-6}	$mol \cdot L^{-1}$
R=	8.3145	$m^3 \cdot Pa \cdot K^{-1} \cdot mol^{-1}$
T=	273.15	K
H_{cc}	2.27	unitless
C_a=	9.23×10^{-6}	$mol \cdot L^{-1}$
C_a=	0.295	$mg \cdot L^{-1}$

Measured sulfate concentrations. As previously mentioned, the NURE groundwater dataset contains sulfate concentrations (SO_4^{2-}) but not concentrations of hydrogen sulfide (H_2S). We investigated possible H_2S concentrations using an equilibrium equation (Equations 4 and 5) between sulfate and hydrogen sulfide which allows calculation of the amount of H_2S present in equilibrium with reported concentrations of sulfate [34]. We also calculated equilibrium concentrations for bisulfide (HS^-)[34]; Equations 6 and 7).

$$SO_4^{2-} + 10H^+ + 8e^- = H_2S(aq) + 4H_2O \quad (4)$$

$$[H_2S(aq)] = K\,[SO_4^{2-}]\,[\,e^-\,]^8\,[H^+]^{10} \quad (5)$$

Where $K = 10^{41}$ [28]

$$SO_4^{2-} + 9H^+ + 8e^- = HS^-(aq) + 4H_2O \quad (6)$$

$$[HS^-(aq)] = K\,[SO_4^{2-}]\,[\,e^-\,]^8\,[H^+]^9 \quad (7)$$

Where $K = 10^{38}$ [38]

Calculations using this equation require a p*e* value, which as previously discussed is a challenging task. Examination of p*e*-pH diagrams for sulfur (Figure S4E, F) and Figures S5 and S6 were used to constrain the best estimate of p*e* for the line between SO_4^{2-} and H_2S [28]. For this calculation we used a pe of −3. Based on the p*e*-pH diagrams (Figure S4E, F), you would expect reduced sulfur in a p*e* range of 5 to −15 and a pH range of 0 to 14. If the environmental condition of a sample is in this range, then the possibility of precipitation of sulfides with cations should be considered.

The total concentration of all sulfur species in these samples is not known. Calculated H_2S concentrations range from 10^{-40} mol/L (10^{-36} mg/L) to 10^{32} mol/L (10^{36} mg/L). Eleven percent of these samples have greater H_2S concentrations than SO_4^{2-} concentrations (Figure S9) and these H_2S concentrations plot from pH 3 to 6.5 indicating that H_2S is likely important to element mobility at lower pH values. HS^- equilibrium concentrations range from 10^{-33} mol/L (10^{-29} mg/L) to 10^{32} mol/L (10^{36} mg/L). Approximately 15% of the HS^- concentrations are greater than the SO_4^{2-} concentrations indicating that HS^- is also likely important to element mobility at lower pH values. Therefore, based on these calculations, reduced sulfur may exist along the Texas Coastal Plain.

Reducing conditions were not identified as a common redox condition along Permissive Tract 3. Since As, Mo, and Se can form sulfides under reducing conditions, the reduced sulfur species may not be a concern for these COPCs in this study area.

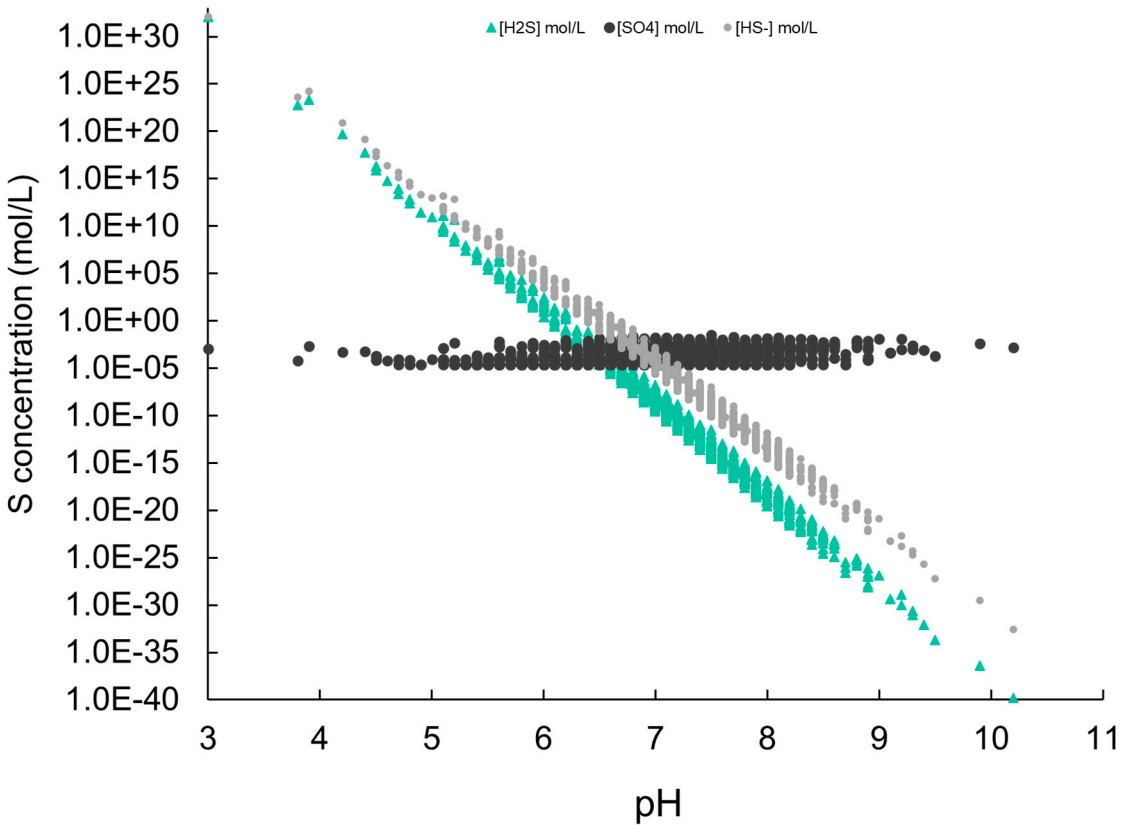

Figure S9. Plot of NURE groundwater SO_4^{2-} concentrations in mol/L versus pH and calculated equilibrium H_2S and HS^- concentrations in mol/L versus pH.

4.2. Neither Sulfate or Hydrogen Sulfide Concentrations or Odor Are Reported

In cases where neither SO_4^{2-} or H_2S concentrations or odor were reported, the p*e*-pH and speciation diagrams were consulted (Figure S4). We noted that the concentrations of total sulfide could be influenced by the precipitation or dissolution of metal sulfides or sulfate-bearing minerals. Recall, in the South Texas Coastal Plain groundwater system, pyrite has been invoked as a possible electron donor that could explain the reductive precipitation of aqueous uranyl ions to form the sandstone hosted uranium deposits [12,35,11]. Considering the Fe-S-H_2O system p*e*-pH diagrams along with the measured range of pH in our datasets and a range of p*e* values (+/−15) in Figure S4G and H, the dominant sulfide solid species is pyrite. However, there may be other sulfide solid species along the South Texas Coastal Plain. Using PHREEQC [36] and equilibrium constants for likely sulfides pyrite (log K= −18.479) and mackinawite (log K= −4.648) and from gypsum, the equilibrium concentrations of H_2S were calculated over the range of p*e* and pH of pyrite stability from Figure S4. If pyrite is present, total dissolved sulfide (as hydrogen sulfide, bisulfide and/or sulfide) could range from 3.11×10^{-4} mg/L (8.47×10^{-9} mol/L) to 165 mg/L (5.1×10^{-3} mol/L) (Table S4). The H_2S concentration could range from 1.28×10^{-6} mg/L (3.76×10^{-11} mol/L) to 0.476 mg/L (1.4×10^{-5} mol/L). Furthermore, sulfate could range from 1.8×10^{-29} mol/L to 1.24×10^{-9} mol/L. When mackinawite is present, total reduced sulfide could range from 0.020 mg/L (6.39×10^{-7} mol/L) to 15.9 mg/L (4.98×10^{-4} mol/L). The equilibrium sulfur concentrations from gypsum are all in the oxidized form.

Table S4. Equilibrium aqueous concentrations of sulfur species from pyrite, mackinawite, and gypsum modeled in PHREEQC.

	pH	p*e*	Total S (mol/L)	Total S (mg/L)	S^{-2} (total of reduced sulfur species) (mol/L)	S^{-2} (mg/L)	H_2S (mol/L)	H_2S (mg/L)	HS- (mol/L)	HS- (mg/L)	SO_4^{2-} (mol/L)	SO_4^{2-} (mg/L)
Pyrite	3	-2	1.41×10^{-5}	4.51×10^{-1}	1.41×10^{-5}	4.51×10^{-1}	1.41×10^{-5}	4.79×10^{-1}	1.68×10^{-9}	5.53×10^{-5}	5.34×10^{-23}	5.13×10^{-18}
	7	0	9.71×10^{-9}	3.11×10^{-4}	8.47×10^{-9}	2.71×10^{-4}	3.86×10^{-9}	1.31×10^{-4}	4.48×10^{-9}	1.48×10^{-4}	1.24×10^{-9}	1.19×10^{-4}
	12	-10	5.15×10^{-3}	1.65×10^{2}	5.15×10^{-3}	1.65×10^{2}	3.76×10^{-11}	1.28×10^{-6}	2.73×10^{-6}	9.02×10^{-2}	1.82×10^{-29}	1.75×10^{-24}
Macki-nawite	3	-2	4.98×10^{-4}	1.59×10^{1}	4.98×10^{-4}	1.59×10^{1}	4.94×10^{-4}	1.68×10^{1}	1.78×10^{-6}	5.87×10^{-2}	1.19×10^{-27}	1.14×10^{-22}
	7	0	6.39×10^{-7}	2.04×10^{-2}	6.39×10^{-7}	2.04×10^{-2}	5.65×10^{-8}	1.92×10^{-3}	4.85×10^{-7}	1.60×10^{-2}	5.07×10^{-17}	4.87×10^{-12}
	12	-10	9.15×10^{-5}	2.93×10^{0}	9.15×10^{-5}	2.93×10^{0}	2.36×10^{-13}	8.02×10^{-9}	2.89×10^{-8}	9.54×10^{-4}	6.23×10^{-26}	5.98×10^{-21}
Gypsum	3	-2	1.59×10^{-2}	5.08×10^{2}	1.77×10^{-6}	5.66×10^{-2}	1.77×10^{-6}	6.01×10^{-2}	4.34×10^{-10}	1.43×10^{-5}	1.03×10^{-2}	9.93×10^{2}
	7	0	1.57×10^{-2}	5.01×10^{2}	0.00×10^{0}	0.00×10^{0}	0.00×10^{0}	0.00×10^{0}	0.00×10^{0}	0.00×10^{0}	1.56×10^{-2}	1.50×10^{3}
	12	-10	1.65×10^{-2}	5.29×10^{2}	2.21×10^{-8}	7.06×10^{-4}	6.22×10^{-17}	2.12×10^{-12}	7.21×10^{-12}	2.38×10^{-7}	1.13×10^{-2}	1.09×10^{3}

In general, the reduced sulfide concentrations indicated by these three evaluations are relatively low, 10^{-6} mol/L, 10^{-40} mol/L and 10^{-8} mol/L, with the exception of the higher concentrations noted in the equilibrium calculations between sulfate and hydrogen sulfide/hydrogen bisulfide and the equilibrium aqueous concentrations of sulfide from mackinawite. The higher H_2S and HS^- equilibrium concentrations occur at pH values lower than 6.5 in this system, which is where sulfide may be a controlling factor on mobility. Therefore, it will be challenging to make broad statements about the effect of reduced sulfur on element mobility given the limited data. However, individual samples or regions can be evaluated on a case-by-case basis.

Figure S10 shows variograms of the correlation between the variance of all paired NURE values and the spatial distance between those paired values for the observed (black line in the top window) and modeled (variogram model; red line in the top window) data as well as the number of sampled value pairs compared to distance between paired values. Figure S11 shows variograms of the correlation between the variance of all Texas Water Development Board paired values and the spatial distance between those paired values for the observed (black line in the top window) and modeled (variogram model; red line in the top window) data as well as the number of sampled value pairs compared to distance between paired values

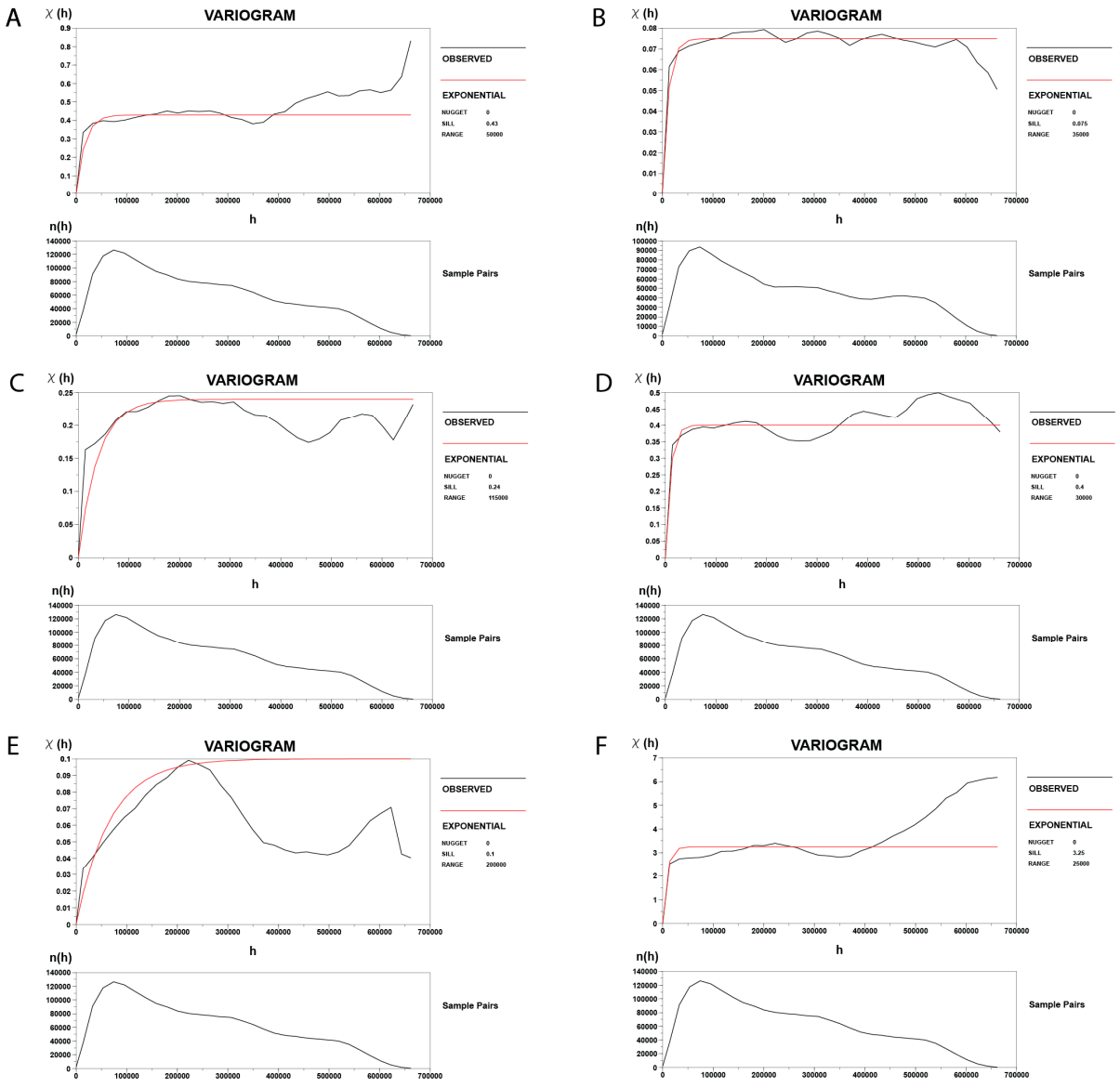

Figure S10. Variograms showing the correlation between the variance of all paired NURE values and the spatial distance between those paired values for the observed (black line in the top window) and modeled (variogram model; red line in the top window) data as well as the number of sampled value pairs compared to distance between paired values (black line in the bottom window) for (**A**) pH, (**B**) DO, (**C**) SO4, (**D**) Mn, (**E**) Fe, and (**F**) S.

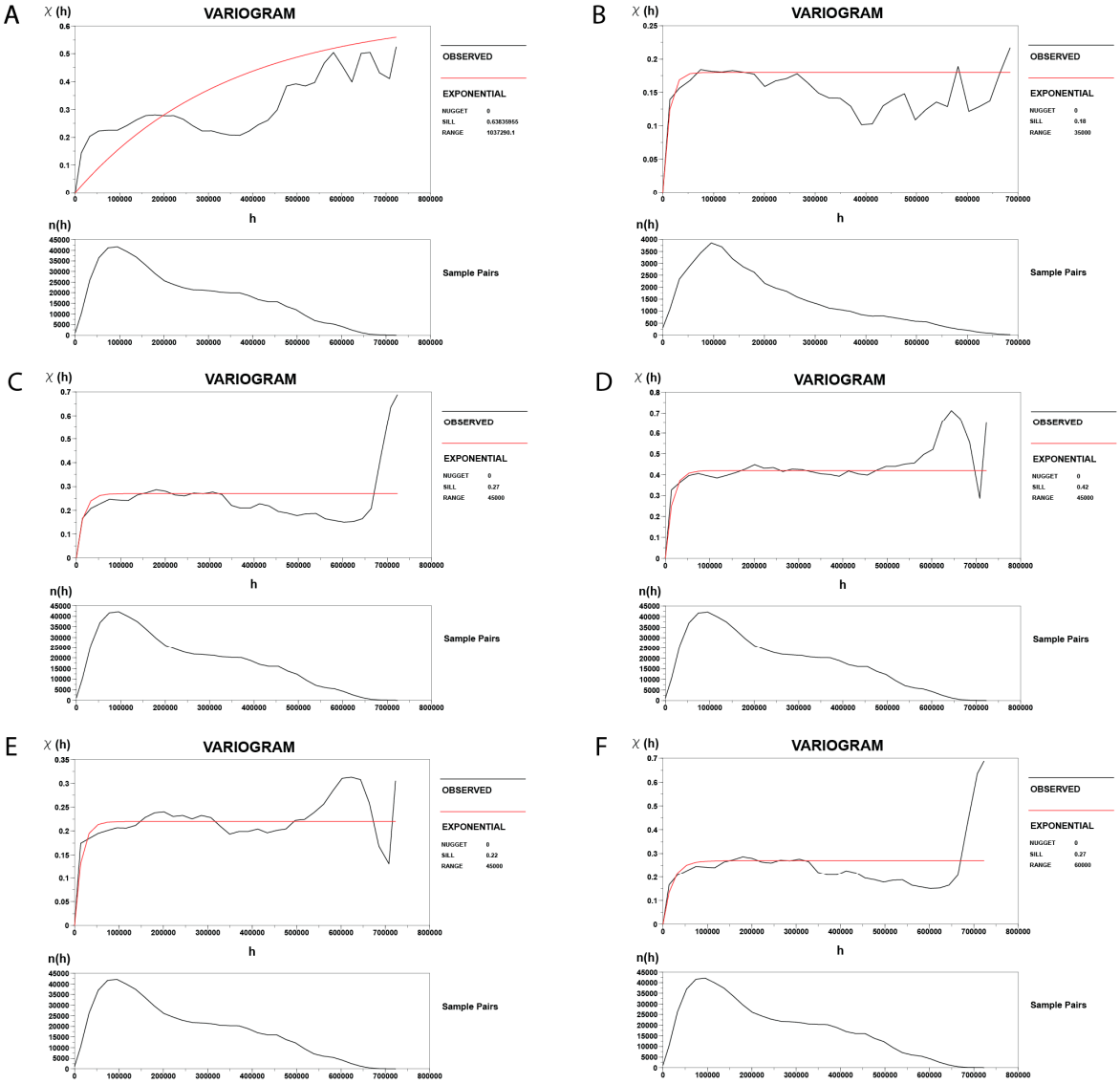

Figure S11. Variograms showing the correlation between the variance of all Texas Water Development Board paired values and the spatial distance between those paired values for the observed (black line in the top window) and modeled (variogram model; red line in the top window) data as well as the number of sampled value pairs compared to distance between paired values (black line in the bottom window) for (**A**) pH, (**B**) DO, (**C**) SO4, (**D**) Mn, (**E**) Fe, and (**F**) S.

The location of data used for Piper diagrams and Piper diagrams of NURE groundwater data are shown in Figure S12.

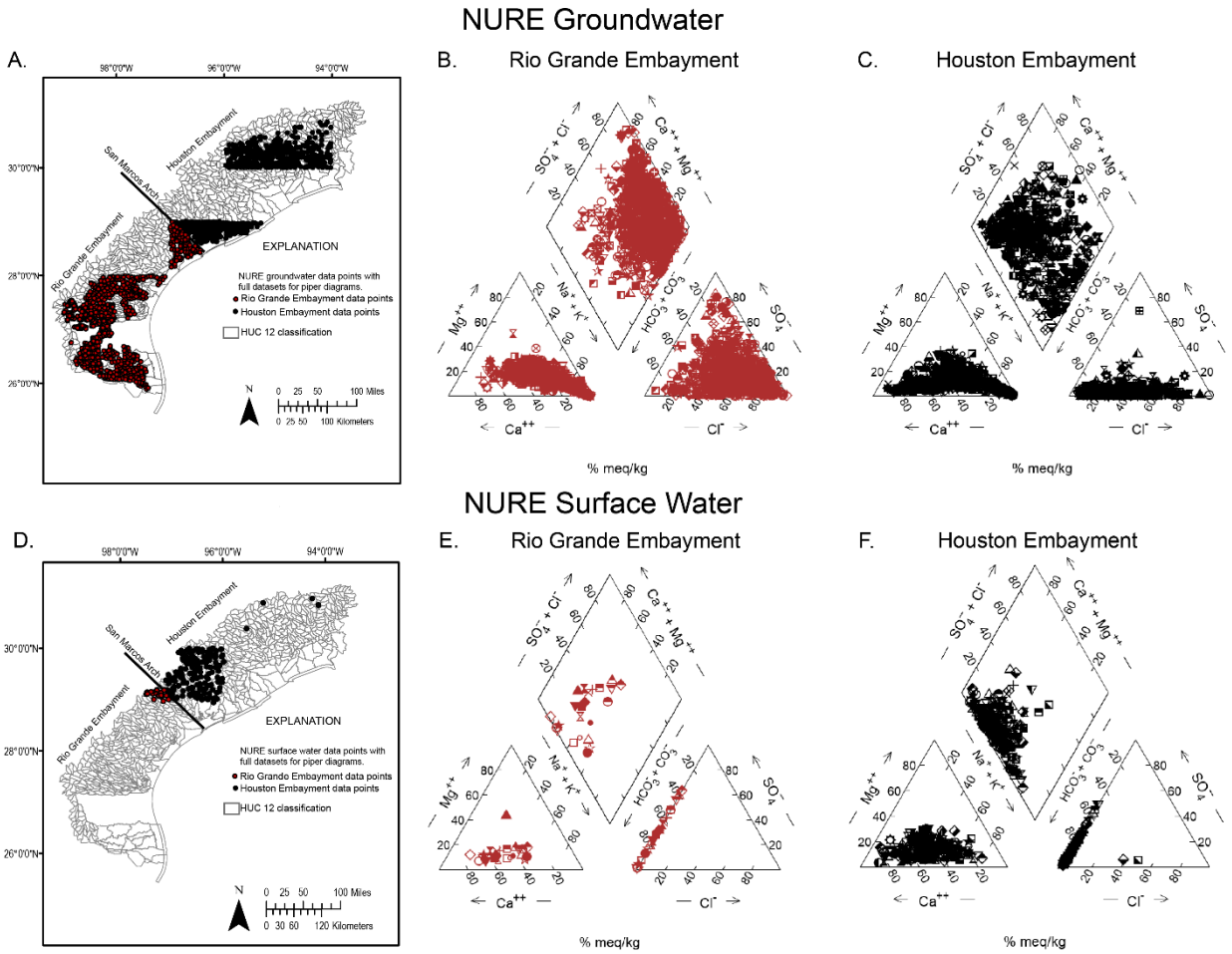

Figure S12. A. Spatial distribution of NURE groundwater points with complete datasets to plot piper diagrams. **B.** Piper diagram of data from the Rio Grande embayment. **C.** Piper diagram of data from the Houston embayment. **D.** Spatial distribution of NURE surface water with complete datasets to plot piper diagrams. **E.** Piper diagram of data from the Rio Grande embayment. **F.** Piper diagram of data from the Houston embayment.

Figure S13 shows the distribution of NURE groundwater COPCs concentrations in micrograms per liter plotted as less than or equal to the detection limit, two times the detection limit, three times the detection limit, four times the detection limit, and samples greater than four times the detection limit. Figure S14 shows the distribution of NURE surface water COPCs concentrations in micrograms per liter plotted as less than or equal to the detection limit, two times the detection limit, three times the detection limit, four times the detection limit, and samples greater than four times the detection limit. Table S5 lists the NURE groundwater constituent of potential concern data compared to the detection limit and Table S6 lists NURE surface water constituent of potential concern data compared to the detection limit. The number of samples greater than the detection limit, the percent of the total sample size greater than the detection limit, and the number of samples in each EC are shown in both Table S5 and S6.

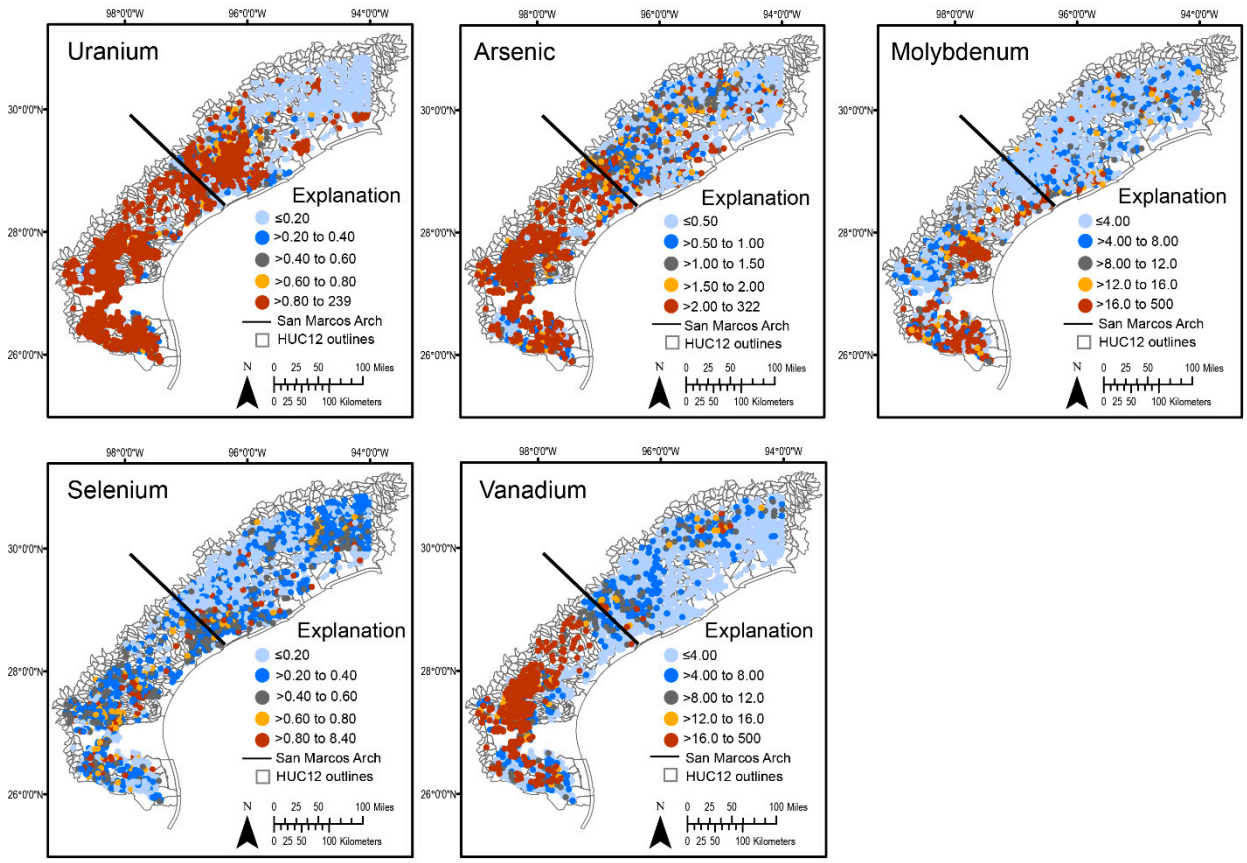

Figure S13. Figures of NURE groundwater COPCs concentrations in micrograms per liter plotted as less than or equal to the detection limit, two times the detection limit, three times the detection limit, four times the detection limit, and samples greater than four times the detection limit.

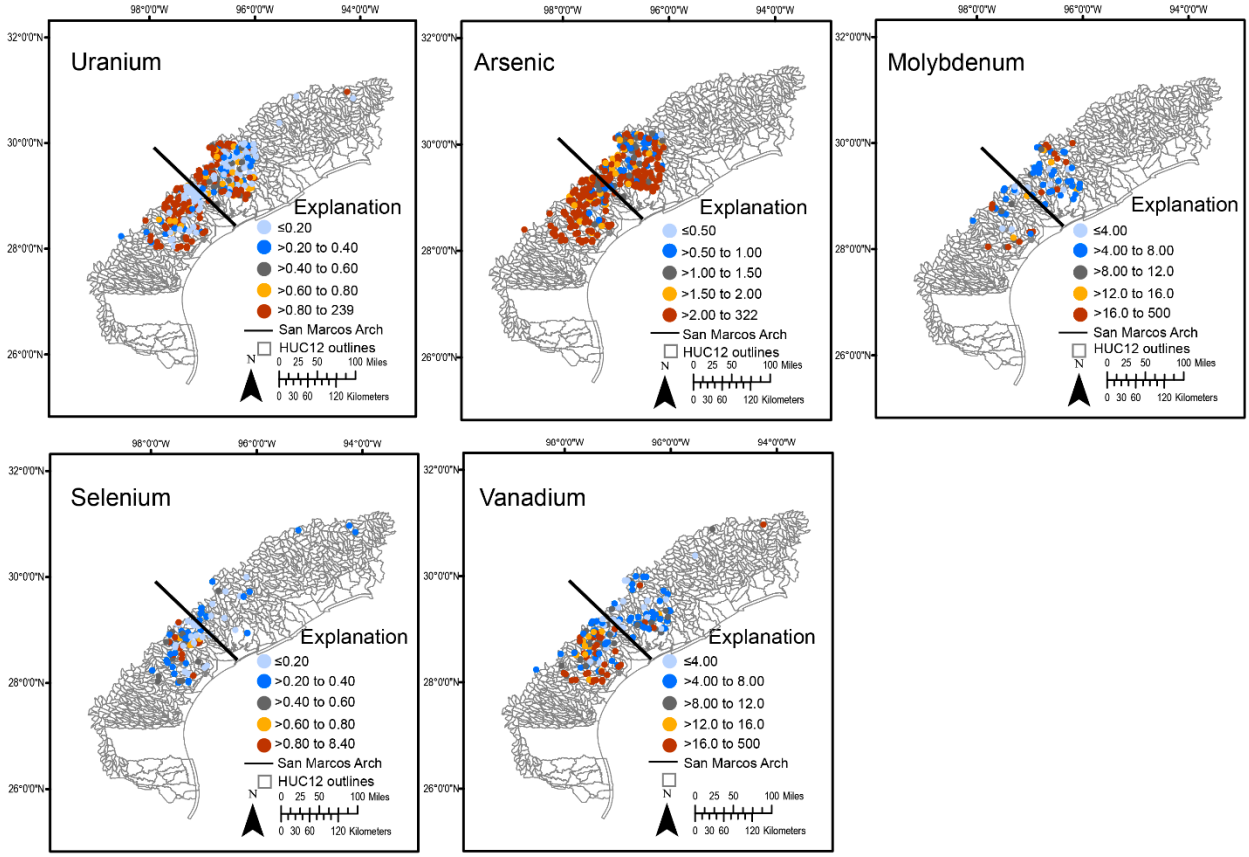

Figure S14. Figures of NURE surface water COPCs concentrations in micrograms per liter plotted as less than or equal to the detection limit, two times the detection limit, three times the detection limit, four times the detection limit, and samples greater than four times the detection limit.

Table S5. NURE groundwater constituent of potential concern data compared to the detection limit. The number of samples greater than the detection limit, the percent of the total sample size greater than the detection limit, and the number of samples in each environmental condition (EC) are shown.

		EC2	EC3	EC4	EC6	EC7	EC10	EC11	EC12
All samples uranium	>0.2	55	1068	31	3	64	18	154	2
	%>0.2	59	79	78	38	65	72	73	67
	n=	93	1349	40	8	99	25	211	3
Houston embayment uranium	n>0.2	19	376	0	0	11	7	71	0
	%>0.2	35	66	0	0	44	58	58	-
	n=	55	572	6	2	25	12	122	0
Rio Grande embayment uranium	n>0.2	34	692	31	1	21	16	115	3
	%>0.2	94	88	89	100	70	89	86	75
	n=	36	785	35	1	30	18	134	4
All samples arsenic	>0.5	54	1132	31	4	66	23	149	2
	%>0.5	26	71	66	44	57	45	55	67
	n=	206	1596	47	9	116	51	273	3
Houston embayment arsenic	n>0.5	30	448	0	1	14	11	77	0
	%>0.5	18	55	0	50	52	28	39	-
	n=	167	809	9	2	27	39	197	0
Rio Grande embayment arsenic	n>0.5	24	688	31	1	26	14	98	2
	%>0.5	62	86	82	100	87	78	73	50
	n=	39	797	38	1	30	18	135	4

All samples molybdenum	>4	36	608	39	1	45	15	129	3
	%>4	17.5	38.1	83	11.1	38.8	29.4	47.3	100
	n=	206	1596	47	9	116	51	273	3
Houston embayment molybdenum	>4	24	204	3	0	7	7	64	0
	%>4	14	25	33	0	26	18	32	-
	n=	167	809	9	2	27	39	197	0
Rio Grande embayment molybdenum	>4	12	407	36	0	10	9	93	4
	%>4	31	51	95	0	33	50	69	100
	n=	39	797	38	1	30	18	135	4
All samples selenium	>0.2	114	993	29	4	73	34	189	3
	%>0.2	55	62	62	44	63	67	69	100
	n=	206	1596	47	9	116	51	273	3
Houston embayment selenium	n>0.2	82	397	5	1	8	30	132	0
	%>0.2	49	49	56	50	30	77	67	-
	n=	167	809	9	2	27	39	197	0
Rio Grande embayment selenium	n>0.2	32	598	24	1	20	8	102	4
	%>0.2	82	75	63	100	67	44	76	100
	n=	39	797	38	1	30	18	135	4
All samples vanadium	>4	59	628	12	3	32	11	40	3
	%>4	29	39	26	33	28	22	15	100
	n=	206	1596	47	9	116	51	273	3
Houston embayment vanadium	>4	42	170	0	1	6	5	12	0
	%>4	25	21	0	50	22	13	6	-
	n=	167	809	9	2	27	39	197	0
Rio Grande embayment vanadium	>4	17	458	12	1	18	7	36	0
	%>4	44	57	32	100	60	39	27	0
	n=	39	797	38	1	30	18	135	4

Table S6. NURE surface water constituent of potential concern data compared to the detection limit. The number of samples greater than the detection limit, the percent of the total sample size greater than the detection limit, and the number of samples in each EC are shown.

NURE surface water constituent of potential concern comparison to the element detection limit in μg/L									
		EC2	EC3	EC4	EC6	EC7	EC8	EC10	EC11
Uranium	>0.2	1	465	46	8	83	8	1	3
	%>0.2	12.5	75.9	70.8	66.7	48.5	50.0	33.3	50.0
	n=	8	613	65	12	171	16	3	6
Molybdenum	>4	0	123	19	3	18	7	1	3
	%>4	0.0	19.6	29.23	25.0	10.4	43.8	33.3	50.0
	n=	11	626	65	12	173	16	3	6
Arsenic	>0.5	3	535	61	6	158	15	1	6
	%>0.5	27.3	85.6	92.4	50.0	91.3	93.8	33.3	100
	n=	11	625	66	12	173	16	3	6
Selenium	>0.2	4	132	14	4	31	1	2	1
	%>0.2	36.4	21.1	21.2	33.3	17.9	6.25	66.7	16.7
	n=	11	625	66	12	173	16	3	6
Vanadium	>4	5	219	42	6	92	8	2	3
	%>4	45.5	35.0	64.6	50.0	53.2	50.0	66.7	50.0
	n=	11	626	65	12	173	16	3	6

Figure S15 shows a comparison of NURE and TWDB groundwater data by environmental condition.

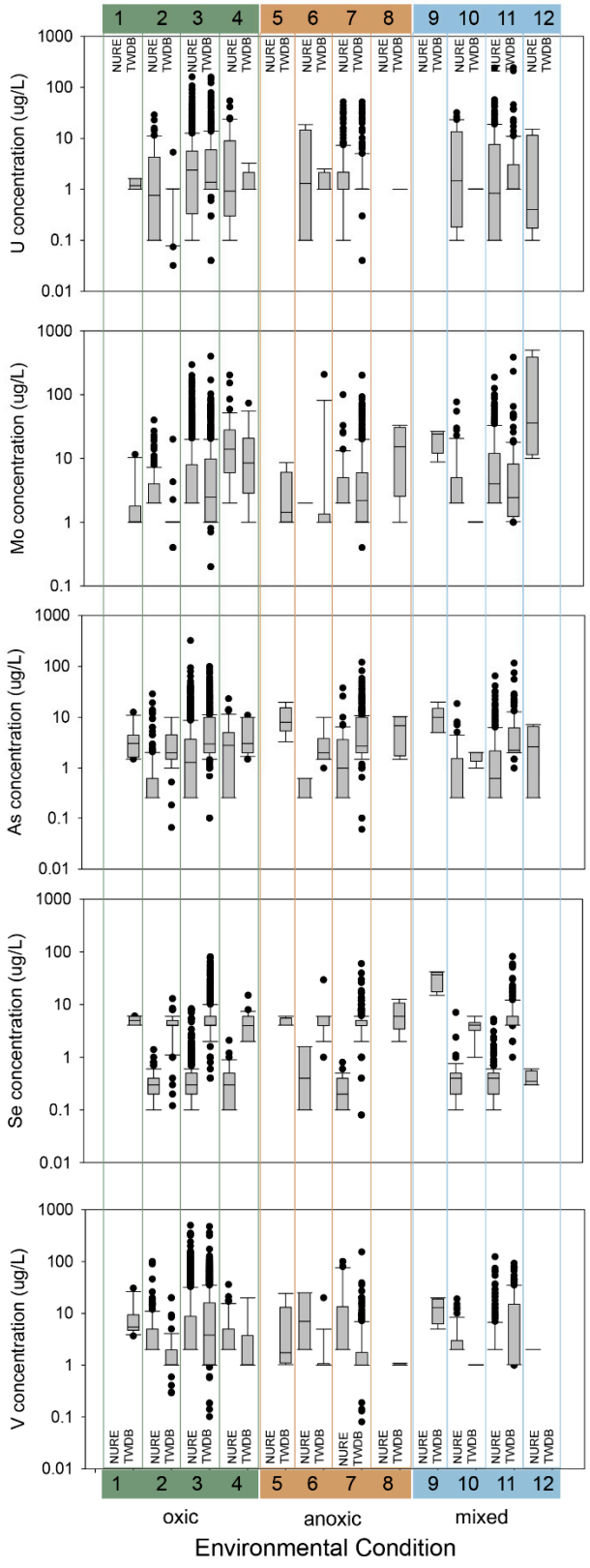

Figure S15. TWDB groundwater data by EC compared to NURE groundwater data by EC.

5. Constituents of Potential Concern Oxidation States and Species

The species and oxidation states of the COPCs were modeled using PHREEQC. Pe values of +11, 0, and −8 were used for oxic, mixed, and anoxic samples, respectively. Results for U, As, and Se can be modeled using the wateq4f database and Mo and V using the minteqv4 database. The ternary complexes that are known to affect U mobility (Stewart et

al., 2010 (37)) were not included in the model but are noted as an important mechanism. A site-specific use of the geochemical framework presented in this study could warrant an evaluation of the U ternary complexes. Results reveal that in the Rio Grande embayment, U(6) was the dominant oxidation state of U for oxic and mixed redox conditions and U(4) was the dominant oxidation state for anoxic redox conditions (Table S7). The dominant oxic and mixed samples species were $UO_2(CO_3)_2^{-2}$ and $UO_2(CO_3)_3^{-4}$ and anoxic samples species $U(OH)_4$.

Table S7. Oxidation state and dominant species for relevant environmental conditions in the Rio Grande embayment.

	Rio Grande Embayment				
	U	**As**	**Mo**	**Se**	**V**
EC2	U(6), $UO_2(CO_3)_2^{-2}$, $UO_2(CO_3)_3^{-2}$	As(5), $HAsO_4^{-2}$, $H_2AsO_4^-$	Mo(6), MoO_4^-	Se(6), $HSeO_3^-$, $SeO4^{-2}$	V(5), $H_2VO_4^-$
EC3	U(6), $UO_2(CO_3)_2^{-2}$, $UO_2(CO_3)_3^{-2}$	As(5), $HAsO_4^{-2}$, H2AsO_4^-	Mo(6), MoO_4^-	Se(6), SeO_4^{-2}	V(5), $H_2VO_4^-$
EC4	U(6), $UO_2(CO_3)_3^{-2}$	As(5), $HAsO_4^{-2}$	Mo(6), MoO_4^-	Se(4), SeO_3^{-2}, HSeO3−	V(5), HVO_4^{-2}, H_2VO4-
EC6	U(4), $U(OH)_4$	As(3), H_3AsO_3	no data	Se(−2)	V(3), $V(OH)_3$
EC7	U(4), $U(OH)_4$	As(3), H_3AsO_3	Mo(6), MoO_4^-	Se(−2),	V(3), $V(OH)_3$
EC10	U(6), $U0_2(CO3)_2^{-2}2$, $U0_2(CO3)_3^{-4}4$, $U0_2CO_3$	As(3), H_3AsO_3	Mo(6), MoO_4^-	Se(−2) and Se(4), $HSeO_3^-$	V(3), $V(OH)_3$
EC11	U(6), $UO_2(CO3)_2^{-2}$, $UO_2(CO3)_3^{-4}$	As(3) and As(5), $HAsO_4^{-2}$, $H_2AsO_4^-$, H_3AsO3	Mo(6), MoO_4^-	Se(4), SeO_3^{-2}, $HSeO_3^-$	V(3), $V(OH)_3$
EC12	U(6), $UO_2(CO_3)_3^{-4}$	As(5), $HAsO_4^{-2}$	Mo(6), MoO_4^-	Se(4), SeO_3^{-2}, $HSeO_3^-$	no data

The PHREEQC modeling of data from the Rio Grande embayment revealed that As(5) was the dominant oxidation state in all of the oxic water samples and 68% of the mixed redox samples. Arsenic 3+ was the dominant oxidation state for the remainder of the mixed redox samples and all of the anoxic samples. The primary species of As modeled in PHREEQC in the oxic samples were $HAsO_4^{-2}$ and $H_2AsO_4^-$. The mixed redox samples have modeled As species of $HAsO_4^{-2}$, $H_2AsO_4^-$, H_3AsO_3, and $H_2AsO_3^-$. The As species of the anoxic samples was primarily as H_3AsO_3.

Results of the PHREEQC model from the Rio Grande embayment reveal that 98% of the oxic and mixed samples had a Se(6+) oxidation state and 2% had a Se(4+) oxidation state. The Se oxidation state of the anoxic samples was Se(−2). The majority of the oxic samples have a primary Se species of SeO_4^{-2}. The primary Se species from the mixed redox samples were $HSeO_3^-$ and SeO_3^{-2}. The primary species of the anoxic samples was HSe-.

References

1. Langmuir, D., Aqueous Environmental Geochemistry. Prentice-Hall, Inc.: Englewood Cliffs, NJ, USA, 1997, p601.
2. DeVore, C.L.; Rodriguez-Freire, L.; Ali, A.M.; Ducheneaux, C.; Artyushkova, K.; Zhou, Z.; Latta, D.E.; Lueth, V.W.; Gonzales, M.; Lewis, J. et al. Effect of bicarbonate and phosphate on arsenic release from mining-impacted sediments in the Cheyenne River watershed, South Dakota, USA. *Environ. Sci. Processes Impacts* **2019**, *21*, 456 –468. DOI: 10.1039/c8em00461g.
3. Kim, M.; Nriagu, J.; Haack, S. Carbonate ions and arsenic dissolution by groundwater. Environmental Science and Technology **2000**, *34(15)*, 3094–3100. DOI: 10.1021/es990949p.
4. Dong, W. M.; Brooks, S. C. Determination of the formation constants of ternary complexes of uranyl and carbonate with alkaline earth metals (Mg^{2+}, Ca^{2+}, Sr^{2+}, and Ba^{2+}) using anion exchange method. *Environ. Sci. Technol.* **2006**, *40 (15)*, 4689−4695.
5. Blake, J.M.; Avasarala, S.; Artyushkova, K.; Ali, A.S.; Brearley, A.J.; Shuey, C.; Robinson, W.P.; Nez, C.; Bill, S.; Lewis, J.; Hirani, C.; Lezama Pacheco, J.S.; Cerrato, J.M. Elevated concentrations of U and co-occurring metals in abandoned mine wastes in a

northeastern Arizona Native American community. Environmental Science & Technology **2015**, *49*, 8506−8514. DOI: 10.1021/acs.est.5b01408.
6. Saunders, J.A.; Pivetz, B.E.; Voorhies, N.; Wilkin, R.T. Potential aquifer vulnerability in regions down-gradient from uranium in situ recovery (ISR) sites. *J. Environ. Manag.* **2016**, *183*, 67–83. DOI: 10.1016/j.jenvman.2016.08.049\.
7. Han, M.; Hao, J.; Christodoulatos, C.; Korfiatis, G.P.; Wan, L.; Meng, X. Direct evidence of arsenic (III)-carbonate complexes obtained using electrochemical scanning tunneling microscopy. *Anal. Chem.* **2007**, *79*, 3615–3622. DOI: 10.1021/ac062244t
8. Jenne, E.A. Adsorption of metals by geomedia: data analysis, modeling, controlling factors, and related issues. In *Adsorption of Metals by Geomedia*, Jenne, E.A. Ed.; Academic Press: Cambridge, Massachusetts, USA, 1998; pp. 1–73.
9. Smith, K.S. Metal sorption on mineral surfaces: An overview with examples relating to mineral deposits. In *Reviews in Economic Geology*, Plumlee, G.S., Logsdon, M.J., Filipek, L.F., Eds.; Society of Economic Geologists: Littleton, CO, USA, 1999; Volumes 6A and 6B, pp. 161–182.
10. Galloway, W.E. Uranium mineralization in a coastal-plain fluvial aquifer system: Catahoula Formation, Texas. *Econ. Geol.* **1978**, *73*, 1655–1676.
11. Reynolds, R.L. and Goldhaber, M. B. Origin of a south Texas roll-type uranium deposit. I. Alteration of iron-titanium oxide minerals. *Econ. Geol.* **1978**, *73*, 1677–1689.
12. Hall, S.M., Mihalasky, M.J., Tureck, K.R., Hammarstrom, J.M., and Hannon, M.T. Genetic and grade and tonnage models for sandstone-hosted roll-type uranium deposits, Texas Coastal Plain, USA, *Ore Geol. Rev.* , **2017**, *80*, 716–753, http://dx.doi.org/10.1016/j.oregeorev.2016.06.013
13. Smith, K.S., 2007, Strategies to predict metal mobility in surficial mining environments, in *Reviews in Engi-neering Geology, Understanding and Responding to Hazardous Substances at Mine Sites in the Western United States*. DeGraff, J.V., ed., Geological Society of America: Boulder, CO, USA, v. XVII, p. 25–45, doi: 10.1130/2007.4017(03).
14. Perel'man, A.I. Geochemical barriers: Theory and practical applications. *Appl. Geochem.* **1986**, *1*, 669–680.
15. Jurgens, B.C., McMahon, P.B., Chapelle, F.H., and Eberts, S.M. An Excel workbook for identifying redox processes in ground water. U.S. Geological Survey Open-File Report 2009–1004. U.S. Geological Survey: Reston, Virginia, USA. 2009.
16. McMahon, P.B., and Chapelle, F.H. Redox processes and water quality of selected principal aquifer systems, Groundwater, **2008**, *46(2)*, 259–271. doi: 10.1111/j.1745-6584.2007.00385.x
17. Smith, S.M., 2006, National Geochemical Database—Reformatted Data from the National Uranium Resource Evaluation (NURE) Hydrogeochemical and Stream Sediment Reconnaissance (HSSR) Program, U.S. Geological Survey Open-file report 97-492, Version 1.41. Available online: https://pubs.usgs.gov/of/1997/ofr-97-0492/nurehist.htm (accessed on 01 January 2022).
18. Walton-Day, K., Macaladay, D.L., Brooks, M.H., and Tate, V.T. Field methods for measurement of ground water redox chemical parameters. *Groundw. Monit. Remediat.* **1990**, *10(4)*, 81–89. Doi: 10.1021/es902194x
19. Wilkin, R.T., McNeil, M.S., Adair, C.J., and Wilson, J.T. Field measurement of dissolved oxygen: A comparison of methods. *Groundw. Monit. Remediat.* **2001**, *21(4)*, 124–132.
20. Price, Van, and Jones, P.L., 1979, *Training manual for water and sediment geochemical reconnaissance*: E.I. du Pont de Nemours & Co., Savannah River Laboratory, Aiken, S.C., SRL Internal Doc. DPST-79-219, U.S. Department of Energy, Grand Junction, Colo., GJBX-420(81), 104 p.
21. Bolivar, S.L. An overview of the National Uranium Resource Evaluation Hydrogeochemical and Stream Sediment Reconnaissance Program, LA-8457-MS, U.S. Department of Energy, Division of Uranium Resources and Enrichment: Washington, WA, USA, 1 July 1980.
22. Grimes, J.G. NURE HSSR Geochemical Sample Archives transfer report Part 3 Geochemical analysis (K/UR--500-Pt3). Oak Ridge Gaseous Diffusion Plant, Ridge Gaseous, TN, USA. July 1984.
23. Hem, J.D. *Study and Interpretation of Chemical Characteristics of Natural Waters. 3rd Edition, US Geological Survey Water Supply* Paper 2254, U.S. Geological Survey: Reston, Virginia, USA, 1989, 363p.
24. Schwertmann, U. and Fitzpatrick, R.W., Iron minerals in surface environments. *Catena Suppl.* **1992**, *21*, p.7–30.
25. Bethke, C. and Farrell, B., 2020, The Geochemist's Workbench Release 14, GWB Reference Manual, Available online: https://www.gwb.com/pdf/GWB14/GWBreference.pdf (Accessed on: 26 September 2020)
26. Kennedy, V.C., Zellweger, G.W., Jones, Blair, F., Filter pore-size effects on the analysis of Al, Fe, Mn, and Ti in Water. *Water Resour. Res.* **1974**, *10*, 4.
27. Grundl, T.J., Haderlein, S., Nurmi, J.T., and Tratnyek, P.B. Chapter 1: Introduction to Aquatic Redox Chemistry *in* Tratneyk et al., *Aquatic Redox chemistry. ACS Symposium Series*; American Chemical Society: Washington, DC, WA, USA. 2011.
28. Stumm, W. and Morgan, J.J. Aquatic Chemistry, 2nd Edition. Wiley Interscience: Hoboken, NJ, USA, 1981, 780 pp.
29. Contreras, C. Historical data review on Garcitas Creek Tidal. Performed as part of the Tidal Stream Use Assessment under TCEQ Contract No. 582-2-48657 (TPWD Contract No. 108287). Resource Protection Division, Texas Parks and Wildlife Department. 2003. Available online: https://tpwd.texas.gov/landwater/water/conservation/coastal_studies/uaa/media/garcitas.pdf (accessed on 15 September 2020).
30. Eargle, D.H., Dickinson, K.A., and Davis, B.O. South Texas Uranium Deposits. *AAPG Bull.* **1975**, *59(5)*, 766-779.
31. Hamlin, H.S., Salt domes in the Gulf coast Aquifer, in Mace, R.E., Davidson, S.C., Angle, E.S., and Mullican, W.F. III., eds. Texas Water Development Board Report 365: Aquifers of the Gulf Coast of Texas. Available online: https://www.twdb.texas.gov/publications/reports/numbered_reports/doc/R365/R365_Composite.pdf (accessed on 01 January 2022).
32. Simonton, S. and Spears, M. Human health effects from exposure to low-level concentrations of hydrogen sulfide. *Occup. Health Saf.* **2007**, *76(10)*,102–104.

33. Sander, R. Compilation of Henry's law constants (version 4.0) for water as solvent, *Atmos. Chem. Phys*. **2015**, *15*, 4399–4981, https://doi.org/10.5194/acp-15-4399-2015, 2015.
34. Hem, J.D. *Study and Interpretation of the Chemical Characteristics of Natural Water*, 2nd Ed.; U.S. Geological Survey: Liston, VA, USA, **1970**; Water Supply Paper 1473.
35. Goldhaber, M.B., Reynolds, R.L., Rye, R.O. Origin of a south Texas roll-type uranium deposit. 2. Sulfide petrology and sulfur isotope studies. *Econ. Geol.* **1978**, *73*, 1690–1705.
36. Parkhurst, D.L.; Appelo, C.A.J. Description of input and examples for PHREEQC version 3—A computer program for speciation, batch-reaction, one-dimensional transport, and inverse geochemical calculations. *U.S. Geological Survey* **2013**. Available online: https://pubs.usgs.gov/tm/06/a43/ (Accessed on 01 March, 2020).
37. Stewart, B.D., Mayes, M.A., and Fendorf, S. Impact of uranyl-calcium-carbonato complexes on uranium(VI) adsorption to synthetic and natural sediments, **2010**, *44*, 928–934.